

Orbital roulette: a new method of gravity estimation from observed motions

Andrei M. Beloborodov^{1,2}, Yuri Levin³

ABSTRACT

The traditional way of estimating the gravitational field from observed motions of test objects is based on the virial relation between their kinetic and potential energy. We find a more efficient method. It is based on the natural presumption that the objects are observed at a random moment of time and therefore have random orbital time phases. The proposed estimator, which we call “orbital roulette”, checks the randomness of the phases. The method has the following advantages: (1) It estimates accurately Keplerian (point-mass) potentials as well as non-Keplerian potentials where the unknown gravitating mass is distributed in space. (2) It is a complete statistical estimator: it checks a trial potential and accepts it or rules it out with a certain significance level; the best-fit measurement is thus supplemented with error bars at any confidence level. (3) It needs no *à priori* assumptions about the distribution of orbital parameters of the test bodies. We test our estimator with Monte-Carlo-generated motions and demonstrate its efficiency. Useful applications include the Galactic Center, dark-matter halo of the Galaxy, and clusters of stars or galaxies.

Subject headings: galaxies: general — stars: stellar dynamics

1. Introduction

Estimation of a central point mass M from measured positions and velocities of its N satellites is a classic problem of astronomy which applies to various gravitating systems. More generally, the gravitating mass is distributed in space with density $\rho(\mathbf{r})$, so that N test bodies move in an unknown potential $\Phi(\mathbf{r})$, and astronomers estimate Φ from the observed motions. In many cases the orbital periods of the test bodies are much longer than the age of modern astronomy and therefore only instantaneous positions and velocities are available rather than the full orbits of the bodies. This does not allow one to find the exact M even in a point-mass problem. Instead, statistical methods are used to obtain an approximate estimate.

Customary methods of mass estimation stem from the virial relation between the mean potential energy and mean kinetic energy. It enables an estimation of Φ from the observed kinetic

¹Physics Department, Columbia University, 538 West 120th Street New York, NY 10027

²Astro-Space Center of Lebedev Physical Institute, Profsojuznaja 84/32, Moscow 117810, Russia

³Canadian Institute for Theoretical Astrophysics, 60 St. George Street, Toronto, ON M5S 3H8, Canada

energy of test bodies. One notes, however, that in a *finite* system of N test bodies, the *instantaneous* relation between their potential and kinetic energies deviates from the virial relation. The variance of such deviations is unknown to the observer because it depends on the unknown orbital parameters of the bodies. For this reason, the observer does not possess a well defined error of the estimated mass.

The virial theorem itself is a statistical statement about the potential and kinetic energies that is based on the presumption that *the observed bodies have random orbital time phases*.¹ Thus, the virial relation is not the original information we possess but a derivative of the random-phase principle. The latter simply states that the time we point our telescope to the system is random from the point of view of each body. One can make use of this basic principle directly, without invoking the virial theorem. In this paper, we follow this approach and develop a new method of potential estimation which we call orbital roulette (because the true orbital phase obeys the same statistics as a fair roulette, see § 3). We show that this method is principally better and in practice more efficient than the virial estimator.

In many applications, the estimation of potential Φ is further complicated by the lack of full 3D information on the positions \mathbf{r}_i and velocities \mathbf{v}_i of test bodies: often only projections on the sky or line-of-sight components are measured. A projected version of orbital roulette will be addressed in a future paper. Here we develop the basic method in its full 3D version and discuss the astronomical data sets to which it is immediately applicable.

The idea of our method is as follows. Consider a point-mass problem with Keplerian potential $\Phi = -GM/r$ and suppose one tries to infer the central mass M from observed motions of its satellites. For any trial mass M_{trial} , the observed positions \mathbf{r}_i and velocities \mathbf{v}_i of the satellites uniquely determine their orbits. Thus, for any M_{trial} , one can find the current orbital phases of the satellites. If M_{trial} is smaller than the true mass M_{true} , the orbital phases will be found near the pericenters, and if $M_{\text{trial}} > M_{\text{true}}$ then the phases will cluster near the apocenters. Only for $M_{\text{trial}} = M_{\text{true}}$ is the orbital roulette unbiased and the calculated phases are randomly distributed between the pericenter and the apocenter. One can therefore figure out M_{true} by checking the randomness of the inferred phases. In § 3, we put this idea on a quantitative basis and show how the lower and upper bounds on M are obtained at a given confidence level.

In § 4 we extend the method to non-Keplerian potentials that have more than one unknown parameter and refine the roulette principle: the inferred orbital phases must be consistent with random numbers *and* uncorrelated with the inferred integrals of motion. This refinement is important for estimation of potentials created by distributed mass.

¹The random-phase condition is satisfied in many astronomical systems including stellar clusters and clusters of galaxies (in planetary systems it may not hold if planets interact with each other and are locked in resonances). The virial relation is evidently not valid if the motions of the test bodies are correlated and the time of observation is chosen so that, for example, all bodies are near their pericenters. We do not consider the case of correlated test bodies here.

One problem in the previously proposed methods was the need for *a priori* assumptions about the test bodies’ population. For instance, Little & Tremaine (1987) and Kochanek (1996) used Bayesian analysis to estimate the mass of our Galaxy. In order to make progress, they needed some assumptions about the Galactic satellites’ distribution function.² The roulette method makes no assumption about the orbits of test bodies. For a trial $\Phi(\mathbf{r})$, it simply reconstructs the orbits and checks the obtained orbital phases. $\Phi(\mathbf{r})$ is deemed a good estimate at a confidence level C if the phases are consistent with random distribution at the confidence level C . This test extracts the maximum information on $\Phi(\mathbf{r})$ one could possibly extract from data.

Any statistical estimator in general should be able to judge a trial gravitational potential $\Phi(\mathbf{r})$ and accept it or rule out with a certain significance. Thus, the allowed hypotheses can be sorted out at a given confidence level. The virial estimator does not work in this way: it gives only a best bet on the mass and a rough guess of its error based on the previous experience with numerical simulations of gravitating systems. One of the advantages of the estimator we propose is its completeness in the sense that it enables derivation of the errors at any given confidence level.

The adequate statistical approach becomes especially valuable when one tries to discriminate between different models of $\Phi(\mathbf{r})$ that have more than one parameter. Consider for example a set of trial models with two parameters p_1 and p_2 . Which model is in best agreement with positions and velocities of the observed bodies? What p_1 and p_2 are allowed at the 90% confidence level? The virial relation is not able to answer such questions. It gives instead a relation between p_1 and p_2 (and an approximate error of this relation). The roulette estimator turns out to be much more powerful: it constrains both p_1 and p_2 at any chosen confidence level. We illustrate this in § 4 with a simple halo model that has two parameters: the halo size b and mass m . In this example, the instantaneous positions and velocities of N test bodies moving in the halo potential contain information on m and b which one would like to extract. The roulette method gives a best fit (m_0, b_0) as well as confidence contours on the (m, b) plane, and we test its efficiency with Monte-Carlo generated sets of bodies in a known potential $(m_{\text{true}}, b_{\text{true}})$. We find that the standard deviation of (m_0, b_0) from the true values is as small as 10-15% for $N = 32$.

The success of the roulette method is partially due to its ability to use the full 3D information on the positions \mathbf{r}_i and velocities \mathbf{v}_i of the test bodies. By contrast, the virial estimator uses only absolute values r_i and v_i ($i = 1, \dots, N$), and thus the angles between \mathbf{v}_i and \mathbf{r}_i are ignored. These angles are quite valuable as they contain information on the eccentricities of the orbits. For instance, if \mathbf{v}_i is parallel to \mathbf{r}_i it is clear that the body is on a radial (linear) orbit, while the virial estimator is not “aware” of that. The advantage of the roulette method in this respect becomes less clear in applications where only projected components of \mathbf{r}_i and \mathbf{v}_i are known from observations. The method then needs to be modified, which is deferred to a future paper. Already in its 3D

²The Bayesian method also makes use of the roulette principle because the satellite distribution function is assumed to depend only on the integrals of motion. This form of the distribution function is justified by the strong Jeans theorem whose proof relies on the randomness of orbital phases (Appendix 4A in Binney & Tremaine 1987).

version, the roulette estimator has useful applications that are briefly discussed in § 5.

2. Virial estimator

In this section, we discuss briefly the performance of the virial estimator applied to N test bodies orbiting a point mass M . It will be used later as a benchmark. The virial theorem states for any bound orbit

$$\left\langle \frac{GM}{r} \right\rangle = \langle v^2 \rangle, \quad (1)$$

where angle brackets signify a time average. The same relation holds for a population of $N \rightarrow \infty$ bodies observed at one moment of time if the average is taken over the population.³ For a set of observed positions r_i and velocities v_i one gets the virial mass

$$M_v = \frac{\sum v_i^2}{G \sum 1/r_i}, \quad i = 1, \dots, N. \quad (2)$$

M_v converges to M_{true} at $N \rightarrow \infty$, independently of the (unknown) orbital eccentricities of the bodies which makes the virial relation tempting for mass estimations. The virial estimator has, however, the following drawbacks:

1. — It does not involve any statistical analysis of the data. Instead of confidence intervals the estimator gives a direct formula for M in terms of observed positions and velocities of the test bodies. For a finite N , M_v is not equal to the true mass, and its mean expectation and variation depend on the unknown orbital eccentricities of the bodies e_i .

This is evident in the extreme case of $N = 1$. Then equation (2) gives $M_v = G^{-1}v^2r$ where v and r are the velocity and radial position of the observed body. The mean expectation for M_v is $\langle M_v \rangle = G^{-1} \langle v^2r \rangle$ where the average is now taken over the ensemble of random realizations of the data set. Each realization can be thought of as a snapshot taken at a random moment of time and $\langle v^2r \rangle$ equals the time-averaged value of v^2r for the true orbit (see Appendix),

$$\langle v^2r \rangle = GM_{\text{true}} \left(1 - \frac{e^2}{2} \right). \quad (3)$$

The standard deviation $\Delta(v^2r)$ can also be calculated,

$$\frac{\Delta(v^2r)}{\langle v^2r \rangle} = \frac{e}{\sqrt{2 - e^2}}. \quad (4)$$

Thus, both $\langle M_v \rangle$ and $\Delta(M_v)$ depend on the unknown e for $N = 1$.

³The virial relation (1) may be invalid if the population has orbits with strongly varying size a , so that $a_{\text{max}}/a_{\text{min}} \rightarrow \infty$ when $N \rightarrow \infty$.

A qualitatively similar dependence takes place for $N > 1$, and therefore it is difficult to derive the error of M_v without additional assumptions about e_i . The error would vanish for circular orbits ($e_i = 0$): each body would be expected to give the same $M = v_i^2 r_i / G$, $i = 1, \dots, N$. In the case of large e_i the error can be significant even if $N \gg 1$ and depends on the radial distribution of the bodies as we discuss next.

2. — Test bodies that are at larger radii contribute to the virial estimator with a smaller weight and those at the smallest radii make the dominant contribution. If N bodies are spread over a significant range of radii, the effective size of the sample is smaller than N , which leads to a relatively large statistical error of the estimated mass.

For illustration, consider a population of orbits with random eccentricity $0 < e < 1$ and semi-major axis $a_{\min} < a < a_{\max}$, and make a simple Monte-Carlo simulation. For each body $i = 1, \dots, N$ we draw randomly e_i , a_i , and the orbital time phase of the body. Thus we create a “data set” $\mathbf{r}_i, \mathbf{v}_i$. We apply equation (2) to the set and obtain M_v , which we can compare with the true M . Repeating this for many randomly drawn data sets we can study the statistics of M_v .

Figure 1 shows the standard deviation of M_v for $N = 10, 100, 1000$. It depends on the ratio a_{\max}/a_{\min} : with increasing a_{\max}/a_{\min} the statistical error of M_v increases. This happens because the bodies at small r (and correspondingly large v) dominate in equation (2), and the data with large r is practically lost.

To avoid this problem one could relate M to $\langle v^2 r \rangle$ instead of equation (2). This relation, however, depends on e_i , even at $N \rightarrow \infty$. For example, for bodies on orbits with equal eccentricities $e_i = e$ one gets (see eq. 3)

$$M = \frac{\langle v^2 r \rangle}{G(1 - e^2/2)}. \quad (5)$$

A projected version of this estimator was proposed by Page (1952) who studied the case of circular orbits ($e = 0$) and by Bahcall & Tremaine (1981) for arbitrary e . The advantage of such estimates is that bodies at different r contribute equally, which gives a nice convergence of the estimated M with increasing N . Nevertheless, the fact that e is unknown still impedes a precise estimate of M even when the exact $\langle v^2 r \rangle$ is known ($N \rightarrow \infty$).

3. — The virial estimator uses only absolute values r_i and v_i and ignores the angles between \mathbf{v}_i and \mathbf{r}_i .

Finally, we note that the virial estimator is inefficient when applied to non-Keplerian potentials. The virial relation for a general potential is given by

$$\sum_{i=1}^N (\mathbf{v}_i^2 + \mathbf{r}_i \cdot \mathbf{f}_i) = 0, \quad (6)$$

where \mathbf{f}_i are the gravitational accelerations of the test bodies. It gives one condition and, if the potential has more than one unknown parameter, the relation is not able to determine them.

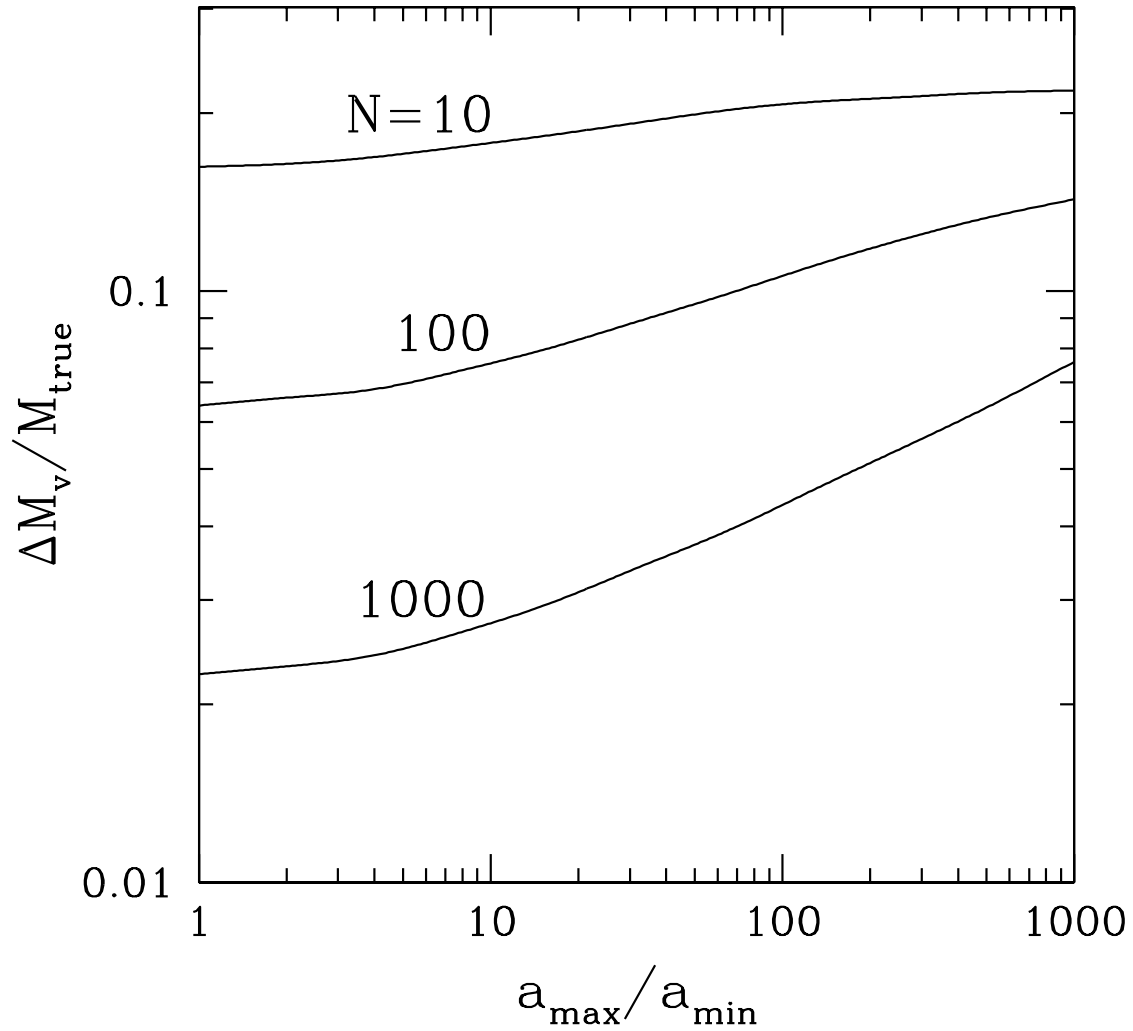


Fig. 1.— Standard deviation of the virial estimate M_v for a point mass with N observed satellites. The orbits of test bodies are assumed to have random orbital eccentricities $0 < e < 1$ and semi-major axes $a_{\text{min}} < a < a_{\text{max}}$.

3. Orbital roulette

Suppose we have measured a current 3D position \mathbf{r} and a velocity \mathbf{v} of a satellite orbiting a central massive object. What can we say about the central mass M based on this “snapshot” information only? First of all, assuming that the satellite is on a bound orbit (its age is longer than the orbital period), we get a lower bound $M_{\min} = v^2 r / 2G$. Then we note that if M is very large, $GM/r \gg v^2/2$, then the satellite has to be extremely close to its apocenter, and if M is small, $M \rightarrow M_{\min}$, it has to be near the pericenter (Fig. 2). The probability of either extreme is low because the snapshot is taken at a random moment of time and, in most cases, the satellite should be somewhere between the pericenter and apocenter. Thus, the requirement of a random orbital time phase can constrain M from above and below at a given confidence level. If we have a snapshot of $N \gg 1$ satellites, the constraint becomes tight. Below we quantify this constraint and develop the mass estimator based on the random-phase principle. The simplest way to check the randomness is by comparing the mean phase with its expected value (§ 3.1) and a more sophisticated method checks the whole distribution of N phases (§ 3.2).

3.1. Mean orbital phase

Let us denote the unknown orbital period of a satellite by T and the time since last passage of the pericenter by t_p . Since we know the current \mathbf{r} and \mathbf{v} , the whole orbit and t_p are unambiguously calculated for any given M_{trial} . For a known orbit, we need a measure of how close the satellite is to the pericenter. We define this measure as time separating the satellite from the nearest passage of the pericenter (in the past or the future) and normalize it by $T/2$,

$$g(M_{\text{trial}}) = \frac{1}{T/2} \begin{cases} t_p & v_r > 0, \\ T - t_p & v_r < 0, \end{cases} \quad (7)$$

so that g can take values between 0 and 1. This definition takes into account that the pericenter is closer in the past if the current radial component of velocity $v_r > 0$, and in the future if $v_r < 0$. The limit $M_{\text{trial}} \rightarrow M_{\min}$ gives $g \rightarrow 0$ (pericenter), and $M_{\text{trial}} \rightarrow \infty$ gives $g \rightarrow 1$ (apocenter). For the true M and a random snapshot time, the expected g obeys Poisson statistics: it has a flat probability distribution between 0 and 1 with the mean expectation value $\langle g \rangle = 1/2$ and the standard deviation $\Delta g = 12^{-1/2}$.

Now suppose we have a snapshot of $N \gg 1$ satellites with measured \mathbf{r}_i and \mathbf{v}_i , $i = 1, \dots, N$. For a given M_{trial} we can calculate the orbit of each satellite and the corresponding $g_i(M_{\text{trial}})$. Then we define the mean phase,

$$\bar{g}(M_{\text{trial}}) = \frac{1}{N} \sum_{i=1}^N g_i(M_{\text{trial}}). \quad (8)$$

Again, $\bar{g} \rightarrow 0$ for small M_{trial} and $\bar{g} \rightarrow 1$ for large M_{trial} . By contrast, for the true M , the expected \bar{g} is described by a narrow probability distribution $f(\bar{g})$ which peaks at $1/2$. At $N \gg 1$, this

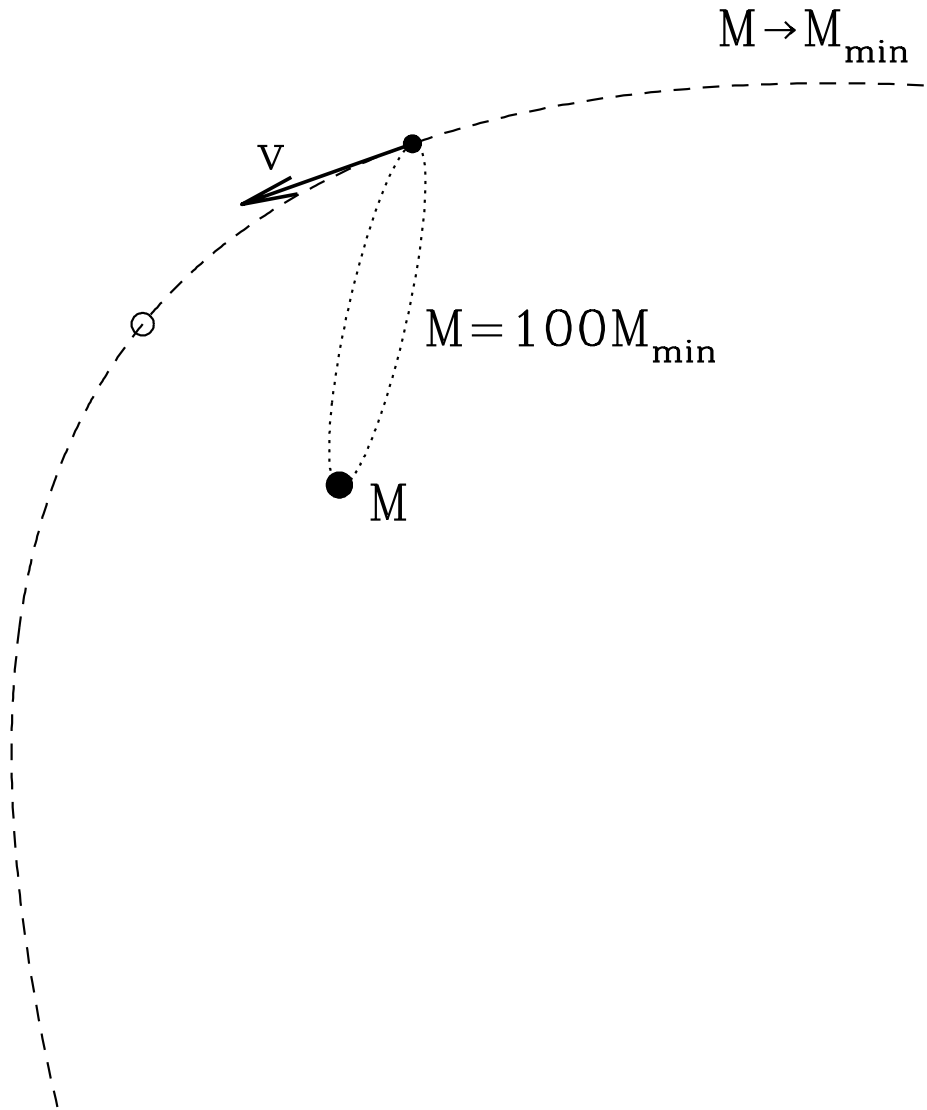


Fig. 2.— Orbit reconstruction for a body with a given position and velocity vector \mathbf{v} . The reconstructed orbit depends on the assumed central mass M . A small $M \rightarrow M_{\min} = rv^2/2G$ gives a large orbit and then the current position is much closer to the pericenter (shown by the open circle) than a distant apocenter far outside the figure. A large M ($100M_{\min}$ in this example) gives a small orbit and places the body almost exactly at the apocenter.

distribution is Gaussian according to the central limit theorem,

$$f(\bar{g}) = \frac{1}{\sqrt{2\pi}\sigma} \exp\left[-\frac{(\bar{g} - 1/2)^2}{2\sigma^2}\right], \quad \sigma = \frac{1}{\sqrt{12N}}. \quad (9)$$

So, one can find the gravitating mass by adjusting M so that

$$\bar{g}(M) = \frac{1}{2} \pm (12N)^{-1/2}. \quad (10)$$

The estimate is well defined since \bar{g} is a monotonic function of M . The width σ of the distribution (9) sets the error of the estimate. Expanding equation (10) near the best-fit point $\bar{g} = 0.5$, one gets the error in M ,

$$\frac{\Delta M}{M} = (12N)^{-1/2} \left[M \frac{d\bar{g}}{dM} \right]_{\bar{g}=1/2}^{-1}. \quad (11)$$

$M(d\bar{g}/dM) = O(1)$ for any large N (variation of M by a factor ~ 2 around the best-fit value induces a change of \bar{g} comparable to $1/2$) and hence $\Delta M/M = O(N^{-1/2})$. The estimate of M defined by equation (10) converges to M_{true} at $N \rightarrow \infty$.

The analysis of orbital phases g_i is similar to testing a roulette wheel. For a fair roulette, the ball angular position on the wheel must be random. Suppose we have a reference position, e.g. Zero, and make N experiments with the roulette. Then we get N random angular deviations from Zero, $0 \leq \alpha_i \leq 180^\circ$, $i = 1, \dots, N$. If the wheel is unbiased, one expects α_i to follow Poisson statistics with a mean value $\bar{\alpha}_i = [0.5 \pm (12N)^{-1/2}] \times 180^\circ$. There is a full analogy with our problem as the magnitude $\bar{g} = \bar{\alpha}/180^\circ$ obeys the same probability distribution (eq. 9). The only difference is that the random variable of orbital roulette is the *time* phase of a test body rather than its angular position.

Equation (10) gives a best-bet value of M and an estimate of its error. We now aim to obtain a more complete solution to the problem: the allowed interval for M at a given confidence level C . Mathematically, this is formulated as follows. For a given number $0 < \xi < 1/2$ we evaluate M_+ such that the probability of $M_{\text{true}} > M_+$ equals ξ , and M_- such that the probability of $M_{\text{true}} < M_-$ equals ξ . The interval $M_-(\xi) < M < M_+(\xi)$ is the mass measurement at the confidence level $C = 1 - 2\xi$.

Let us define cumulative distributions

$$P_-(g) = \int_0^g f(\bar{g})d\bar{g}, \quad P_+(g) = \int_g^1 f(\bar{g})d\bar{g}. \quad (12)$$

$P_- + P_+ = 1$ for any M_{trial} . Then define $g_-(\xi)$ and $g_+(\xi)$ so that

$$P_-(g_-) = \xi, \quad P_+(g_+) = \xi. \quad (13)$$

Note that g_\pm are unique functions of ξ (they depend only on N as a parameter) and the snapshot data \mathbf{r}_i and \mathbf{v}_i did not appear in the definitions (12,13). The data determine $\bar{g}(M)$ and appear in the final equation for $M_\pm(\xi)$,

$$\bar{g}(M_-) = g_-, \quad \bar{g}(M_+) = g_+. \quad (14)$$

One can prove that M_{\pm} defined in this way give the correct confidence interval for M at the confidence level $C = 1 - 2\xi$. Consider the ensemble of all possible snapshots of our test bodies taken at random moments of time. For each snapshot one has $M_-(\xi)$ defined in equation (14). What is the fraction of “bad” snapshots with $M_{\text{true}} < M_-(\xi)$, outside the confidence interval? For these snapshots,

$$\bar{g}_{\text{true}} \equiv \bar{g}(M_{\text{true}}) < g_-(\xi), \quad (15)$$

[this is equivalent to $M_{\text{true}} < M_-(\xi)$ because $\bar{g}(M)$ is a monotonic function for any snapshot]. The probability to get a snapshot with $\bar{g}_{\text{true}} < g_-$ is $P_-(g_-)$, and it equals ξ by definition of g_- . Hence, the probability of a snapshot with $M_{\text{true}} < M_-(\xi)$ equals ξ . Analogously, one shows that the probability of a snapshot with $M_{\text{true}} > M_+(\xi)$ equals ξ .

$P_-(\bar{g}) \ll 1$ signals $M_{\text{trial}} < M_{\text{true}}$, and $P_+(\bar{g}) \ll 1$ signals $M_{\text{trial}} > M_{\text{true}}$. The best bet for M is defined by $P_-(M) = P_+(M) = 1/2$, which is equivalent to $\bar{g}(M) = 0.5$. The best bet is supplemented with the confidence intervals (M_-, M_+) at any confidence level, which also gives an explicit probability distribution of M ,

$$p(M) = \frac{dP_-}{dM} = -\frac{dP_+}{dM} = \frac{d\bar{g}}{dM} f(\bar{g}[M]). \quad (16)$$

This probability distribution is the measurement of M with the mean-phase method.

3.2. Cumulative distribution of orbital phases

When the trial mass is close to M_{true} , the inferred phases g_i should be consistent with a Poisson distribution, which can be used as a test for M_{trial} . Such a test has the advantage of using the whole distribution of g_i rather than just the average \bar{g} . Consider, for example, g_i half of which equal 0 and the other half equal 1. This is clearly inconsistent with a Poisson distribution, yet \bar{g} has the right value of 1/2 and the mean-phase method will not notice the inconsistency.

Testing a distribution for consistency with an expected/model distribution (null hypothesis) is a standard problem of mathematical statistics. It is done by comparing the corresponding cumulative distributions. (Kolmogorov 1941). The cumulative distribution of a given set g_i ($i = 1, \dots, N$) is a stepped function, $0 \leq F(g) \leq 1$, that increases by $1/N$ at each g_i . The null hypothesis in our case is a Poisson process, which gives the mean expectation $\langle F(g) \rangle = g$ at any g (and for any N). Random realizations of the Poisson set g_i have $F(g)$ fluctuating around $\langle F(g) \rangle$ with a binomial distribution,

$$p[F(g)] = \frac{N!}{(FN)!(N - FN)!} g^{FN} (1 - g)^{N - FN}, \quad (17)$$

$$\langle F(g) \rangle = g, \quad \text{Var}[F(g)] = \Delta^2[F(g)] = \frac{g(1 - g)}{N}, \quad (18)$$

where $\text{Var}[X]$ and $\Delta[X]$ denote variance and standard deviation of X . The unknown mass M should be adjusted so that the cumulative distribution of $g_i(M)$ is consistent with a Poisson process.

One then needs a measure of the difference between the obtained $F(g)$ (which depends on M as a parameter) and the mean expectation $\langle F(g) \rangle = g$. The simplest measure would be the Kolmogorov-Smirnov test: one defines $V_{\text{KS}} = \max |F(g) - g|$, where the maximum is searched over the whole interval $0 \leq g \leq 1$ (Kolmogorov 1941). The probability distribution of V_{KS} is known for a true Poisson process (e.g., Press et al. 1992) and getting the actual V_{KS} far in the tail of this distribution signals a low probability of consistency with the null hypothesis.

The Kolmogorov-Smirnov measure is most sensitive to the values of $F(g)$ at median $g \sim 0.5$ where $\text{Var}[F(g)]$ is largest (see eq. 18). In our case, a measure sensitive at the tails $g \approx 0$ and $g \approx 1$ would be preferable because, when M_{trial} deviates from M_{true} , g_i cluster near 0 or 1. We therefore use a different measure

$$V = \int_0^1 \frac{[F(g) - \langle F(g) \rangle]^2}{\text{Var}[F(g)]} dg = N \int_0^1 \frac{[F(g) - g]^2}{g(1-g)} dg. \quad (19)$$

It gives more weight to the tails and is known as the Anderson-Darling test (Anderson & Darling 1952). It can be viewed as χ^2 for a fit of $F(g)$ by $F = g$. Equation (19) becomes the usual formula for χ^2 if the integral is replaced by a finite sum over $dg = 1/K$ with $K \rightarrow \infty$.

The probability distribution of V for a true Poisson process can be calculated numerically by the Monte-Carlo technique. We randomly generate many Poisson sets g_i ($i = 1, \dots, N$), calculate V for each set, and find the histogram of V . The found probability distribution $p(V)$ is shown in Figure 3. It does not depend on N as long as $N \gg 1$. At $V > 2$ ($p < 0.1$) the distribution is very well approximated by a simple empirical formula,

$$p(V) = 10^{-V/2}, \quad V > 2. \quad (20)$$

Having $g_i(M_{\text{trial}})$ and their V , one can quantify the inconsistency of the trial with a Poisson process. The significance level of inconsistency,

$$\xi(V) = \int_V^\infty p(V') dV', \quad (21)$$

is the probability that V' computed for a random Poisson set g'_i is greater than V . A low ξ means that it is unlikely to draw occasionally a Poisson set g'_i with V' as large as our V , and so our M_{trial} is rejected at the significance level ξ .

For $V(M) > 2$, one can use equation (20) to get a simple explicit formula

$$\xi(V) = \frac{2}{\ln 10} 10^{-V/2}, \quad V > 2. \quad (22)$$

All M_{trial} that give $V(M_{\text{trial}}) > -2 \log_{10}[(\xi/2) \ln 10]$ are rejected at the significance level ξ .

The function $V(M_{\text{trial}})$ may be non-monotonic (especially near its minimum), and a number $k \geq 2$ of mass intervals might be rejected. M_{true} belongs to the remaining regions at the confidence

level $C = 1 - k\xi$. In practice, however, our Monte-Carlo simulations show that the case $k > 2$ rarely occurs for ξ of practical interest, and we count only two rejected intervals that cover the tails of low mass (M_{\min}, M_-) and high mass (M_+, ∞). M_{true} belongs to the interval (M_-, M_+) at confidence level $C = 1 - 2\xi$.

3.3. Practical algorithm

We summarize now the practical steps to derive the central point mass M from data. Given a measured position \mathbf{r} and velocity \mathbf{v} of a test body, one first determines its orbital phase g as a function of M . An explicit formula for g is derived in Appendix A,

$$g = \frac{1}{\pi} (2\psi - e \sin 2\psi), \quad (23)$$

where

$$\cos 2\psi = \frac{1}{e} \left(1 + \frac{2Er}{GM} \right), \quad (24)$$

and the orbital energy E and eccentricity e are expressed in terms of \mathbf{r} , \mathbf{v} , and unknown M in Appendix A (eqs. 33,34). Equation (23) gives $g_i(M)$ for each test body $i = 1, \dots, N$.

The mean-phase variant of the roulette estimator is simplest to apply. It defines the best-fit M by equation $\bar{g}(M) \equiv \sum g_i/N = 1/2$. Since \bar{g} increases monotonically with M , only one solution to equation $\bar{g}(M) = 1/2$ can exist. The solution is easily found with the bisection method. The initial interval (M_{\min}, M_{\max}) for bisection can be chosen as follows. M_{\min} is given by the condition that all N orbits are bound: $M_{\min} = \max(v_i^2/2Gr_i)$. M_{\max} should be taken sufficiently large, so that $\bar{g}(M_{\max}) > 1/2$. Note that no solution exists if $\bar{g}(M_{\min}) > 1/2$. It may happen in rare cases where the observed bodies accidentally cluster near their true apocenters and $\bar{g}(M_{\text{true}})$ is large. Such snapshots may have $\bar{g}(M_{\min}) > 1/2$, and then the best-fit mass is not defined by the mean-phase estimator. Only confidence intervals should be considered in this case.

The confidence intervals provide the most useful information. They show the allowed interval for M at a given confidence level $C = 1 - 2\xi$ where ξ can be chosen at any small value. In practice, measurements at the 90% confidence level are often considered, which corresponds to $\xi = 0.05$. Confidence intervals (M_-, M_+) derived with the mean-phase estimator are given by equation (14) where $g_{\pm}(\xi)$ are defined by equations (12,13). Note that $f(\bar{g})$ is precisely Gaussian only for $N \gg 1$, and at small N one should use a different formula: the convolution of N constant functions $f_1(g) = 1, 0 < g < 1$ (the convolution approaches Gaussian quickly with increasing N ; e.g. at $N = 5$ the Gaussian approximation is already good).

The test for the cumulative distribution of orbital phases is slightly more complicated, however, it has the advantage of utilizing all the available data. For any trial mass M one can calculate the

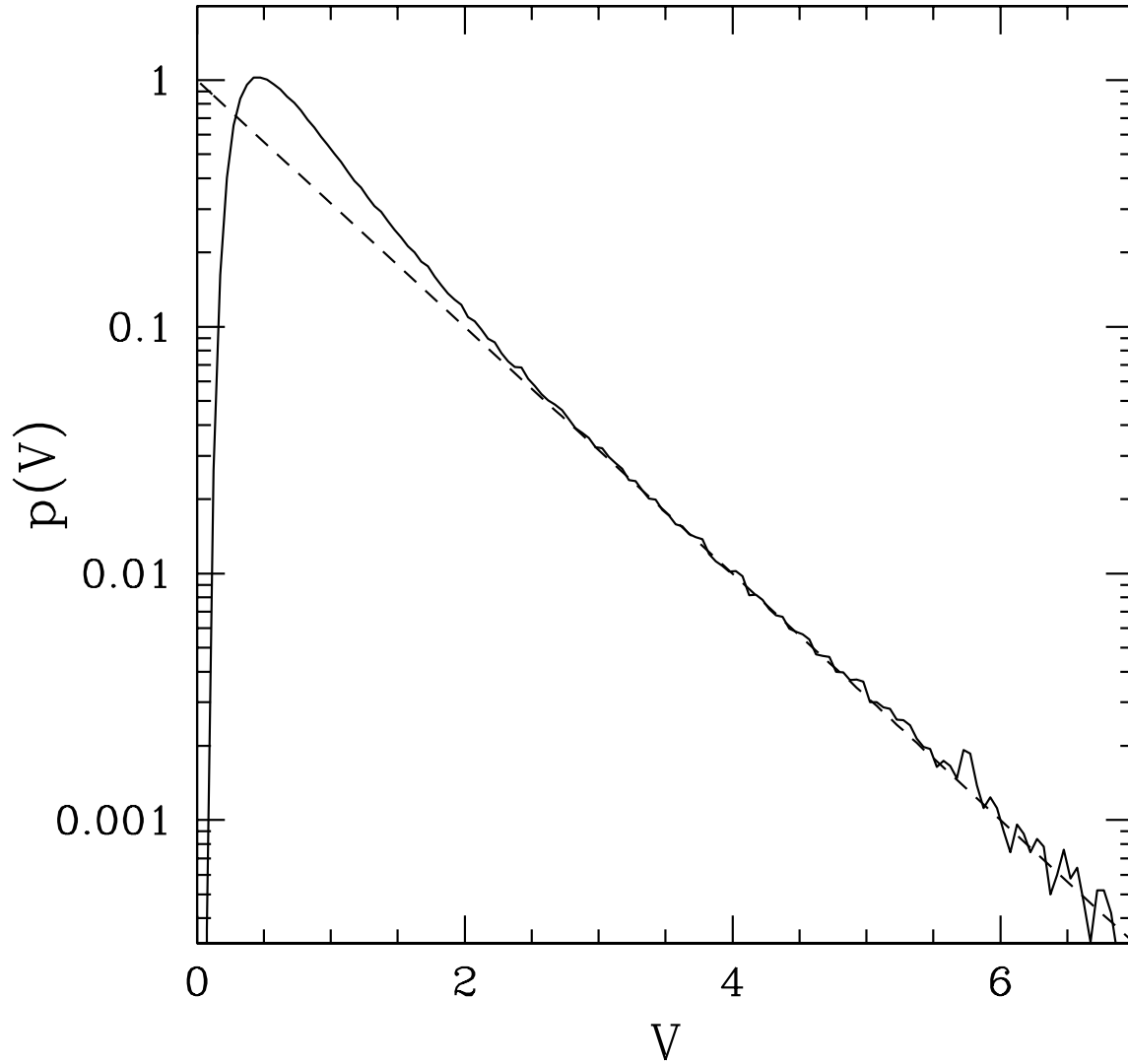


Fig. 3.— Distribution of V (eq. 19) for a true Poisson process with $N \gg 1$. The solid curve shows the result of numerical (Monte-Carlo) calculation. The dashed line shows the approximation $p(V) = 10^{-V/2}$, which is valid at $V > 2$ ($p < 0.1$).

Anderson-Darling $V(M)$ (eq. 19), which can be written as

$$V = N \sum_{i=0}^N \left[\left(\frac{i}{N} \right)^2 \ln \frac{g_{i+1}}{g_i} - \left(1 - \frac{i}{N} \right)^2 \ln \left(\frac{1 - g_{i+1}}{1 - g_i} \right) + g_i - g_{i+1} \right]. \quad (25)$$

Formal $g_0 \equiv 0$ and $g_{N+1} \equiv 1$ are used in this expression. The best-fit M is such that $V(M)$ is minimal. This minimum can be found numerically. Alternatively, one solves the algebraic equation $dV/dM = 0$, which can be written down analytically. The derivative dV/dM is

$$\frac{dV}{dM} = \frac{1}{N^2} \sum_{i=1}^N \frac{dg_i}{dM} \left[\frac{2(N-i)+1}{1-g_i} - \frac{(2i-1)}{g_i} \right], \quad (26)$$

and the expression for dg/dM is derived in Appendix A. This gives an explicit analytical form to equation $\frac{dV}{dM}(M) = 0$. The equation may, however, have many roots, i.e., $V(M)$ may have many local minima and maxima around the global minimum. Therefore in practice it is easier to find the minimum numerically.

Once $V(M)$ is evaluated, one should find the intervals of M that can be rejected at a given significance level ξ as explained in the end of § 3.2. If $\xi < 0.1$ (i.e. the estimate is done on a confidence level $C = 1 - 2\xi > 80\%$), the analytical approximation to $V(\xi)$ can be used. Then the boundaries of the rejected intervals are solutions of the equation $V(M) = -2 \log_{10}[(\xi/2) \ln 10]$.

3.4. Handling data uncertainties

The described method is easy to apply to a snapshot of N bodies with precisely measured \mathbf{r}_i and \mathbf{v}_i . Real data, however, have uncertainties. Suppose a measurement gives 3D distributions $p(\mathbf{v}_i)$ and $p(\mathbf{r}_i)$ rather than numbers \mathbf{v}_i and \mathbf{r}_i ; for example, they may be Gaussian distributions whose widths represent the measurement errors of \mathbf{r}_i and \mathbf{v}_i . Then, for a given M_{trial} , the orbital parameters of the bodies are also described by probability distributions. As a result one obtains N probability distributions $p_i(g_i)$ and $p(\bar{g})$ instead of numbers g_i and \bar{g} .

The $p(\bar{g})$ found for M_{trial} should be compared with the expected distribution $f(\bar{g})$ (eq. 9) and their consistency should be evaluated. This can be done using the Kolmogorov-Smirnov or Anderson-Darling tests. In practice, it is easier to use the Monte-Carlo technique that incorporates the data uncertainties directly in the roulette test for M_{trial} . In each Monte-Carlo event, one draws randomly \mathbf{v}_i and \mathbf{r}_i from the measured distributions $p(\mathbf{v}_i)$ and $p(\mathbf{r}_i)$, calculates the orbits, and finds the mean orbital phase \bar{g} of the N satellites. Then one compares \bar{g} with \bar{g}' for N randomly drawn numbers $0 < g'_i < 1$. Repeating this comparison for many Monte-Carlo \mathbf{v}_i , \mathbf{r}_i and \bar{g}' , one finds the probability $P_-(M_{\text{trial}})$ that $\bar{g} > \bar{g}'$ and the corresponding $P_+(M_{\text{trial}}) = 1 - P_-$. Thus, one gets the same estimator as the one described in § 3.1 but now it allows for the data uncertainties. The best-fit mass is found from the condition $P_- = P_+ = 1/2$ and the confidence intervals are found from $P_- = P_+ = \xi$. In the case of large data uncertainties, the functions $P_{\pm}(M_{\text{trial}})$ are modified and the range of M consistent with the data becomes larger.

The mass estimator based on the Anderson-Darling test of the cumulative distribution of g_i is modified in a similar way to incorporate the data uncertainties.

In a separate paper on the Galactic Center, we present an analysis of a real data set and demonstrate how the measurement errors are taken into account.

3.5. Numerical tests

We now check the performance of the roulette estimator by direct Monte-Carlo simulations. With this purpose, we have developed a numerical code that calculates the best-fit mass and confidence intervals with both mean-phase and cumulative-distribution variants of the estimator.

First of all we check that the confidence intervals are correct. We take N bodies orbiting a central mass M_{true} with randomly chosen eccentricities and semi-major axes. Each body is taken at a random moment of time. This gives us a simulated data set to which we apply the estimator and obtain the 90% confidence intervals (M_-, M_+) . We repeat this procedure for many generated data sets and count the number of cases where M_{true} is outside our confidence interval. These cases should make 10% and we have checked that this is indeed so.

Then we compare the roulette method with the virial estimator. Since the virial estimator does not give confidence intervals, we have to restrict the comparison to the best-fit values of M . We denote them by M_r and M_v for the roulette and virial estimators, respectively. Computer-generated random data sets allow us to study the statistics of M_r and M_v .

The advantage of the roulette estimator becomes significant when the generated orbits have significantly different sizes. For illustration, we draw random semi-major axes of the orbits from an interval $0 < a < a_{\text{max}}$. We also draw a random eccentricity $0 < e < 1$ for each orbit. Each generated data set of N bodies is analyzed with three methods: (1) virial, (2) roulette mean-phase test, and (3) roulette cumulative-distribution test. The results of analysis of 10^5 data sets are shown in Figure 4. We observe that for $N \geq 4$ the roulette method gives a more precise estimate of M than the virial estimator and shows a much faster convergence to M_{true} with increasing N . We also observe that the mean-phase estimator works practically as well as the more complete analysis of the cumulative distribution.

The roulette method is illustrated in Figure 5 for six randomly selected data sets with $N = 10$. The best-fits and 90% confidence intervals obtained with the two roulette estimators strongly correlate with each other.

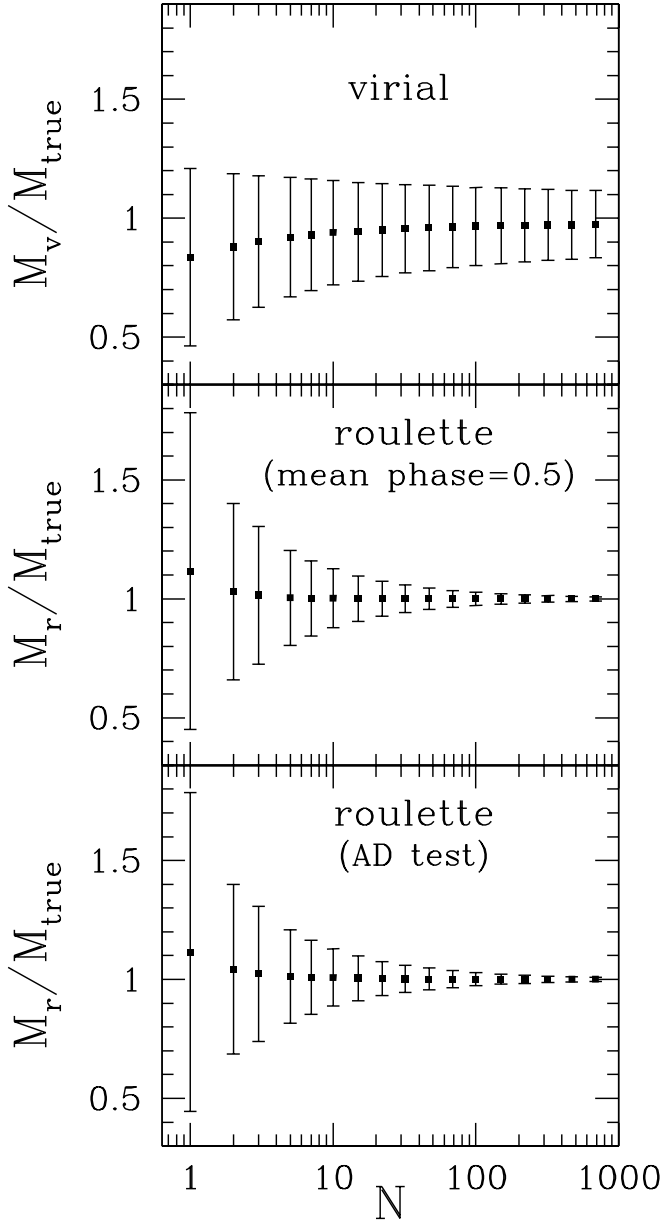


Fig. 4.— Performance of the virial and roulette estimators tested with N bodies on orbits with random eccentricities $0 < e < 1$ and semi-major axes $0 < a < a_{\text{max}}$. The mean value and standard deviation of the estimated mass are shown in the figure as a function of N . Two versions of the roulette estimator are shown: the mean-phase method and the Anderson-Darling (AD) test for the cumulative distribution of phases.

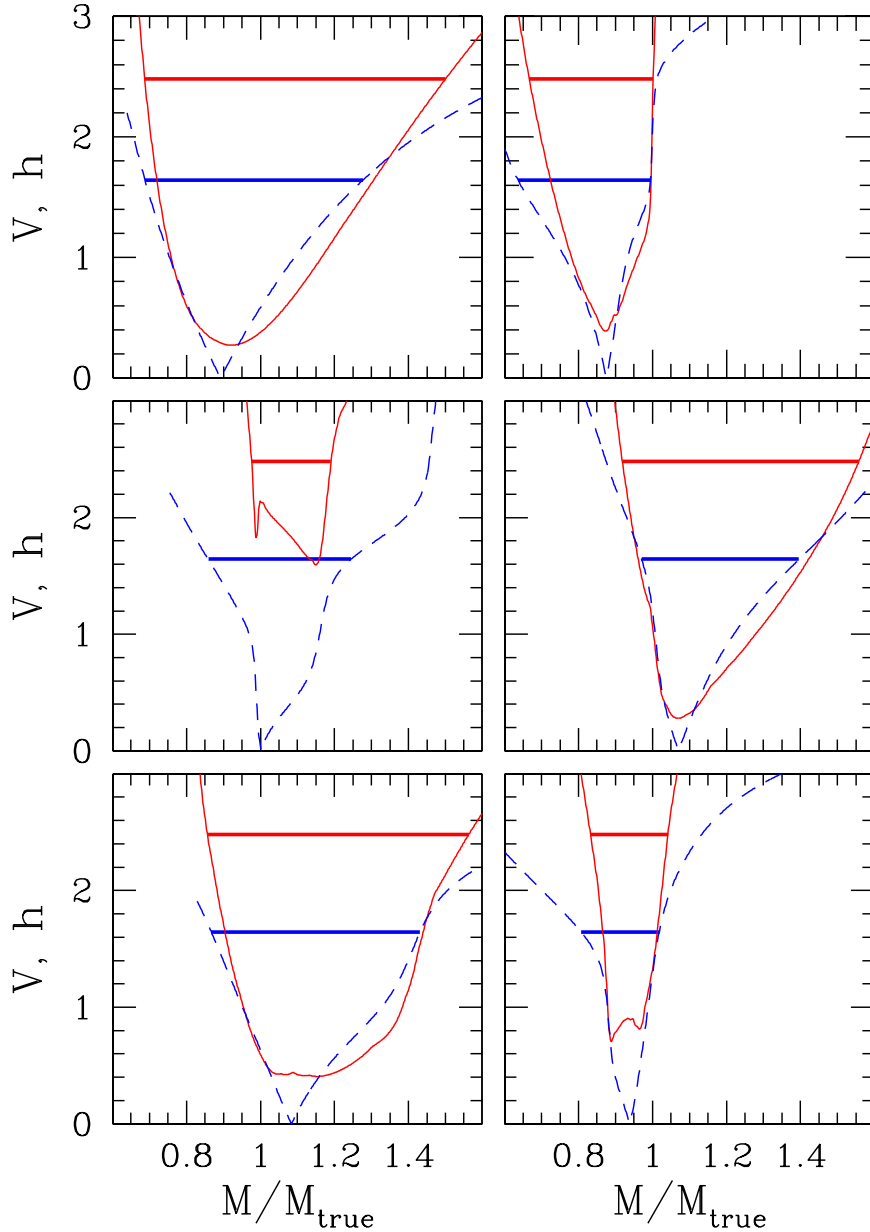


Fig. 5.— Roulette analysis of six randomly selected data sets with $N = 10$ from the sample in Figure 4. Each panel displays the results for one data set. The measure V of the cumulative-distribution estimator is found as a function of trial mass M and shown by solid curve. The minimum of $V(M)$ gives the best-fit M , and $V = 2.48$ defines the 90% confidence interval for M (shown by the horizontal line). The mean-phase estimator compares $\bar{g}(M)$ with $1/2$, and the dashed curve shows $h = |\bar{g} - 0.5|(12N)^{1/2}$ as a function of trial M . Then the best-fit is where $h = 0$, and the 90% confidence interval is defined by $h = 1.643$ ($0.35 < \bar{g} < 0.65$).

4. The case of distributed mass

Suppose we observe N bodies moving in an unknown potential $\Phi(\mathbf{r})$ which is created by a distributed mass with an unknown density profile. Hereafter for brevity we call the gravitating mass “halo” (keeping in mind a dark-matter halo of a galaxy) but it could also be a stellar cluster or a cluster of galaxies. We need only assume that the cluster has a sufficient number of members, so that gravity fluctuations due to motions in the cluster average out, a quasi-steady $\Phi(\mathbf{r})$ is well defined, and each observed body moves on a well-defined bound orbit in this potential. We now apply the roulette method to estimate $\Phi(r)$.

We limit our consideration to spherically symmetric potentials; then an orbital motion is always confined to a plane. Bound orbits in a potential $\Phi(r)$ are not closed in general, however, they still have well-defined pericenter r_1 and apocenter r_2 . The bodies move periodically from the pericenter to the apocenter and back with a period T . This “radial” period is in general not equal to the period of the azimuthal motion. A typical example of such an orbit is a rosette: a superposition of radial oscillations and azimuthal precession (e.g. Binney & Tremaine, 1987).

Since r_1 and r_2 are well defined for each orbit, a moving body has a well defined orbital phase g : the time of motion from the current radius r to the nearest pericenter (in the past or in the future) divided by half period, $T/2$. If the body is observed at a random moment of time then the phase should be a random number $0 < g < 1$ and we can apply the roulette test.

Any trial model $\Phi(r)$ can be tested as it gives certain phases g_i to the observed bodies $i = 1, \dots, N$. The model is good if g_i are consistent with the Poisson distribution, which can be checked in exactly the same way as it was done for point-mass potentials in § 3. In this way, the roulette test sorts out good models $\Phi(r)$ from bad ones.

In practice, one deals with a parametrized family of potentials assuming a certain functional shape of $\Phi(r)$. Estimating $\Phi(r)$ is then reduced to constraining the allowed range of a small number of parameters. The parametrization is consistent with the data if it passes the roulette test with some set of parameters. The test will signal if the assumed parametrization of $\Phi(r)$ is far from reality: the model will not be able to produce Poisson phases if N is sufficiently large. For example, a point-mass model with one parameter M will not give Poisson g_i if the bodies actually move inside a homogeneous halo. Thus, the roulette method checks the assumed parametrization and simultaneously finds the best-fit parameters. In concrete problems, one may have an idea of the possible functional shape of the potential. For example, dark-matter halos are expected to have certain shapes predicted by cosmological simulations of structure formation (e.g. Navarro, Frenk, & White 1996).

For the illustrative purpose, we consider below a simple potential with two parameters b and m ,

$$\Phi(r) = -\frac{Gm}{b + (r^2 + b^2)^{1/2}}. \tag{27}$$

This is the well-known isochron potential (see e.g. Binney & Tremaine 1987); it describes a gravitating mass m distributed in space so that most of it resides inside the characteristic radius b . The corresponding mass density is given by the Poisson equation $\text{div } \Phi = 4\pi\rho$. At $r \ll b$, the density is $\rho \approx \text{const} = (3/16\pi)(m/b^3)$. At $r > b$ the density falls off quickly and $\Phi(r)$ tends to the point-mass potential $\Phi(r) = -Gm/r$. The equation of motion in the isochron potential can be integrated analytically and the orbit shape can be found (see Appendix B).

4.1. Phase-energy correlation

Let us test the efficiency of the roulette estimator with Monte-Carlo generated sets of N test bodies moving in an isochron potential. The true potential has known parameters m_{true} and b_{true} . We assume in this test that the bodies have random orbital energy $E_0 < E < 0$ and random eccentricity $0 < e < e_{\text{max}}$ defined in Appendix.⁴ The minimum $E_0 = -(Gm_{\text{true}}/2b_{\text{true}}) = \Phi_{\text{true}}(0)$ corresponds to a body at rest at $r = 0$, and $e_{\text{max}}(E) = 1 - E/E_0$ is the maximum eccentricity for an orbit with a given E .

The created data set is studied by the roulette estimator which does not know m_{true} , b_{true} . The estimator calculates the orbital phases $g_i(m, b)$ and compares them with the Poisson distribution using the Anderson-Darling measure V as described in § 3. Then it finds the best fit (m_0, b_0) where $V(m, b)$ has a minimum.

We, however, know m_{true} and b_{true} and can check the accuracy of the obtained estimate (m_0, b_0) . This check is made in Figure 6 (upper panel) for 300 simulated data sets with $N = 32$. We plot the results in the q - m plane, where $q = m^{1/3}/b$ is a density parameter. The choice of q and m as two independent parameters (instead of b and m) has a reason that will become clear below.

One can see relatively large deviations of (q_0, m_0) from $(q_{\text{true}}, m_{\text{true}})$. Interestingly, the deviations are concentrated in an elongated region in the q - m plane and their origin can be understood. First, we note that a wrong choice of m affects mostly g_i of bodies at $r > b$, and a wrong choice of q affects g_i of bodies at $r < b$. Consider, for example, $m > m_{\text{true}}$. The orbital phases of the bodies at $r > b$ are then biased to the apocenter. This can be compensated if we choose $q < q_{\text{true}}$: then the bodies at $r < b$ will be biased to the pericenter. Thus, $m > m_{\text{true}}$ and $q < q_{\text{true}}$ can give the correct $\bar{g} = 1/2$ even when they deviate significantly from m_{true} and q_{true} . The total distribution of g_i is then biased to *both* apocenter and pericenter, and there is a lack of intermediate $g_i \sim 1/2$. At large N , the Anderson-Darling test notices such a non-Poisson distribution of g_i and rules out (q, m) that are far from $(q_{\text{true}}, m_{\text{true}})$. With increasing N , the acceptable (q, m) converge to the true values. However, this convergence is relatively slow.

This problem is general for estimations of distributed-mass potentials that have more than

⁴More precisely, we assume in this example a Poisson probability distribution for $\sqrt{-E}$ between 0 and $\sqrt{-E_0}$ and a Poisson distribution for e between 0 and e_{max} .

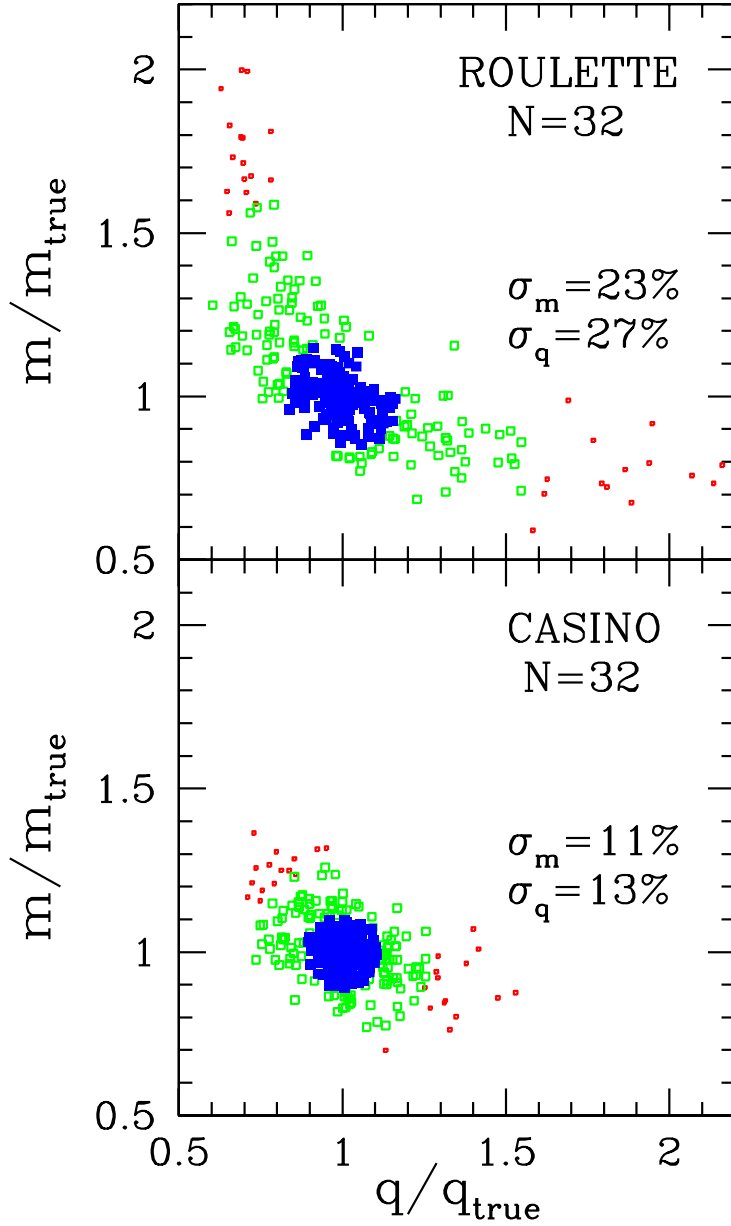


Fig. 6.— 300 best fits to the isochron potential probed with $N = 32$ bodies randomly drawn from a population with random orbital energy and eccentricity (see the text). The fits are shown in the $q - m$ plane where $q = m^{1/3}/b$; m and b are the mass and size of the isochron halo (eq. 27). (a) Roulette method (AD test). (b) Casino method. 10% worst points are in red, 50% best points are in blue, and 40% intermediate points are in green.

one parameter: there are directions in the parameter space where $\bar{g} = 1/2$ is satisfied and the non-flatness of the g_i distribution has to be detected in order to rule out false parameters. The non-flatness is more difficult to detect than a deviation of \bar{g} from $1/2$ because of a lower signal-to-noise ratio, and therefore larger N are required to estimate the potential accurately.

Fortunately, there is an efficient way to avoid this problem and improve the accuracy of the roulette estimator. Indeed, we note that the large deviations of (q_0, m_0) from $(q_{\text{true}}, m_{\text{true}})$ are accompanied by a strong intrinsic correlation between E_i and g_i . In our example above, $m_0 > m_{\text{true}}$ and $q_0 < q_{\text{true}}$, the bodies on small orbits (small E) are found near the pericenter and the bodies on large orbits (large E) are near the apocenter. The orbital energy E_i is an unknown integral of motion (the other integral, angular momentum $\mathbf{l}_i = \mathbf{r}_i \times \mathbf{v}_i$, is known from the data), and our observation can be generalized as follows: large deviations of the best-fit parameters from the true values occur when the orbital phases and unknown integrals of motion are adjusted in a special way and show an intrinsic correlation. Real, truly random, g_i should show no correlation with integrals of motion. Thus, the roulette method can be improved by tracking this correlation and making sure it is absent for the best fits. In particular, in our halo problem, we should track the $E - g$ correlation.

A standard way to detect a monotonic (positive or negative) correlation is to calculate the cross-correlation coefficient $\sum(E_i - \bar{E})(g_i - \bar{g})$. We will use a better measure that would signal any type of correlation between g_i and E_i . First we express the problem mathematically in a convenient way. Given g_i and E_i we can sort the bodies in two ways: by g and by E . Let us denote their phase and energy numbers by i and j , so that $g_{i+1} > g_i$ and $E_{j+1} > E_j$. The absence of correlation between E and g means that the permutation $i \rightarrow j$ is random. This permutation can be viewed as a mixing of N cards (bodies), and in a fair card game we expect a truly random mixing. Plotted on the $i - j$ plane, a random permutation $j(i)$ is represented by a set of N points that should be consistent with a homogeneous 2D distribution in the square $(1, N) \times (1, N)$. Inhomogeneity would signal a correlation.

The consistency with homogeneity can be checked as follows. Consider one point $i, j(i)$. It divides the square into four quadrants: (1) $i' < i, j' < j$, (2) $i' < i, j' > j$, (3) $i' > i, j' < j$, (4) $i' > i, j' > j$. Denote the number of points that fall into each quadrant as N_1, N_2, N_3, N_4 . For a random mixing $j(i)$ the mean expectation values for these numbers are proportional to the areas of the corresponding quadrants. Only one of the four numbers is independent, which we choose to be N_1 (we have $N_2 = i - 1 - N_1$, $N_3 = j - 1 - N_1$, and $N_4 = N - i - N_3 = N - i - j + 1 + N_1$). Random mixings $j(i)$ give the hypergeometric probability distribution for N_1 with the mean expectation value and variance,

$$\langle N_1 \rangle = (j - 1) \frac{(i - 1)}{(N - 1)}, \quad \text{Var}(N_1) = \frac{(N - i)}{(N - 2)} (i - 1) \frac{(j - 1)(N - j)}{(N - 1)^2}. \quad (28)$$

N_1 is consistent with random mixing if its deviation from $\langle N_1 \rangle$ is comparable to $[\text{Var}(N_1)]^{1/2}$.

The inconsistency is measured by

$$V_c[i, j(i)] = \frac{(N_1 - \langle N_1 \rangle)^2}{\text{Var}(N_1)}. \quad (29)$$

Finally we define a measure that should signal deviations from a homogeneous distribution in any part of the square $(1, N) \times (1, N)$,

$$V_c = \sum_{i=2}^{N-1} V_c[i, j(i)]. \quad (30)$$

V_c plays the same role for the card test [randomness of mixing $j(i)$] as the Anderson-Darling measure V played for the roulette test (randomness of phase g_i). Using the Monte-Carlo technique we have calculated numerically the statistics of V_c for truly random card mixings. We thus have the probability distribution of V_c , its mean expectation $\langle V_c \rangle$, and variance $\text{Var}(V_c)$. A mixing $j(i)$ with some V_c will not pass our card test at a significance level ξ if the probability that a fair $V'_c > V_c$ equals ξ .

4.2. Casino

For the true potential $\Phi_{\text{true}}(r)$ we should have random orbital phases g_i and random energy-phase mixing $j(i)$. Thus we expect to deal with a fair casino,

$$\text{fair casino} \equiv \text{fair roulette} + \text{fair cards}. \quad (31)$$

For a false trial potentials $\Phi(r)$ we will detect that its casino is unfair by looking at the combination,

$$\chi^2(\Phi) = \frac{V^2}{\text{Var}(V)} + \frac{V_c^2}{\text{Var}(V_c)}. \quad (32)$$

Our best bet for $\Phi(r)$ is the potential that minimizes χ^2 .

A fair casino has a certain cumulative probability distribution $P(\chi^2)$ which we have calculated numerically. It is shown in Figure 7. For example, one can see from the figure that a model that gives $\chi^2 \approx 16$ is good with 90% confidence (10% significance of inconsistency with the null hypothesis of fair casino). Using $P(\chi^2)$ one can sort out acceptable potentials at any given confidence level.

Let us illustrate the efficiency of the casino method by applying it to the isochron potential. We repeat our Monte-Carlo simulation shown in the upper panel of Figure 6, but now we get the best fit by minimizing χ^2 rather than V . The results are shown in the lower panel of Figure 6. The accuracy of the casino estimator is improved significantly compared with the simple roulette. The standard deviations of the best fits from $(q_{\text{true}}, m_{\text{true}})$ are now 11-13%, and 90% of the best fits show deviations less than $\sim 25\%$.

We think that the casino method extracts completely the available information from the data and does the best estimate of Φ that could possibly be done. As an illustration, we show in Figure 8

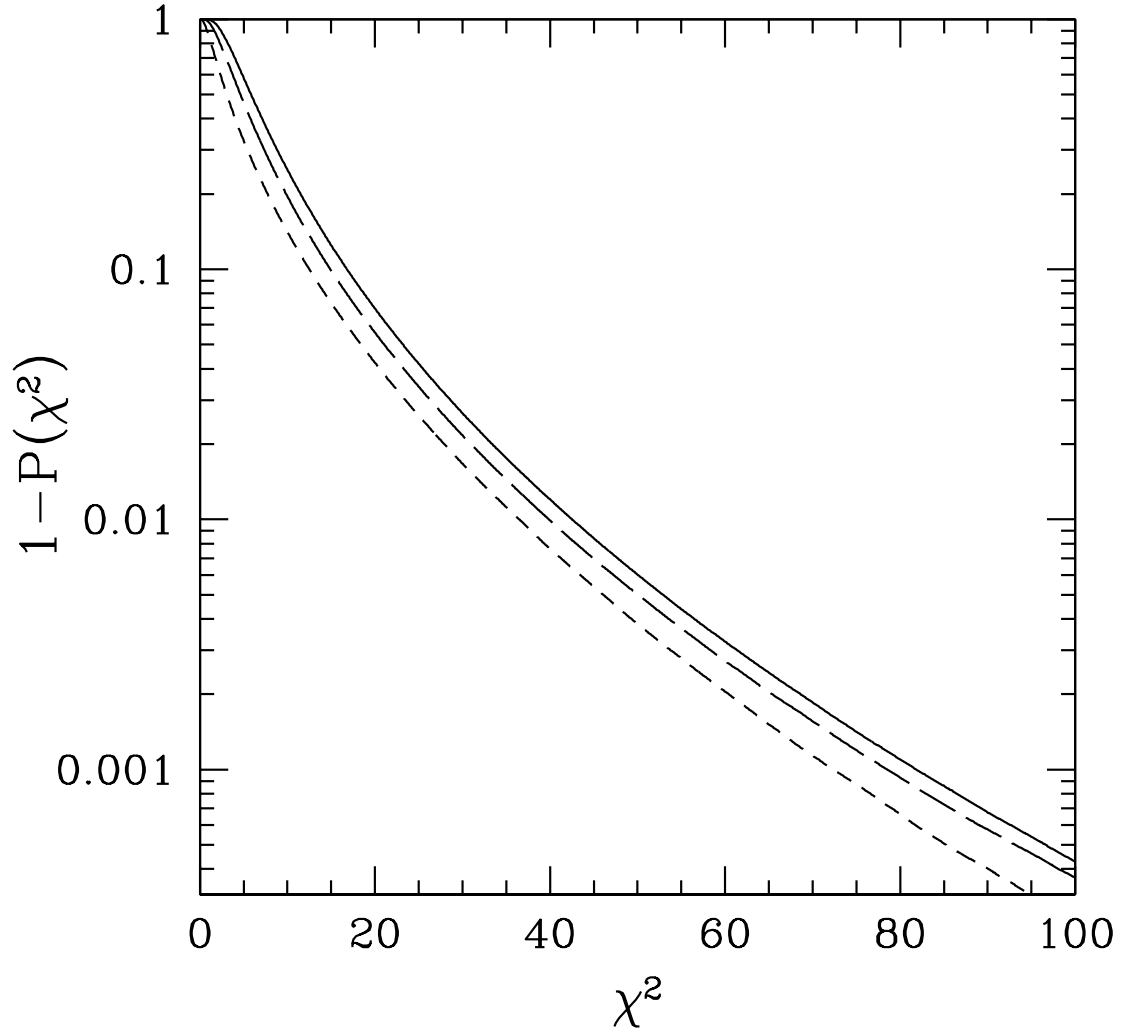


Fig. 7.— Cumulative distribution of the casino measure χ^2 defined in equation (32). Short-dashed, long-dashed, and solid curves show the cases $N = 10, 32,$ and $100,$ respectively.

the results of the method application to three Monte-Carlo-generated data sets with $N=100$. In a similar way, it would be applied to real data. The only difference is that here we know the true potential (and the method does not). The results are presented as 90% confidence area on the $q-m$ plane. The data set analyzed in panel (a) is drawn from a population with random orbital energy E between 0 and $E_0 = -(Gm_{\text{true}}/2b_{\text{true}})$ and random e . It gives a compact confidence area and both q and m are correctly measured with accuracy better than 10%. Panel (b) shows the result for a data set with E randomly drawn from the interval $E_0 < E < (19/20)E_0$. In this case, the bodies sit well inside b and the method cannot say anything about the total mass of the halo m . This is evident for us because we know m_{true} and b_{true} , so we know that the bodies are inside b . However, the method initially did not know that. It finds that it cannot say anything about m and hence *finds* that the observed bodies move in a central part of a distributed mass. It measures well (with 4% accuracy) all it could possibly measure: the central density $\rho = (3/16\pi)q^3$. Panel (c) shows the case where E is drawn from the interval $E_0/20 < E < 0$. Here the dominant majority of the bodies are far outside b and the method measures well the total mass m but cannot say anything about b and ρ . Thus it finds that the test bodies move in essentially a point-mass potential and estimates this mass with accuracy better than 10%.

We have also checked the method ability to reject incorrect parametrizations of $\Phi(r)$. For example, if the test bodies move inside a homogeneous halo, $N = 10 - 15$ is enough to reject the point-mass model: the best-fit then has too high χ^2 and does not pass the casino test. The confidence level of rejection increases quickly with N .

5. Discussion

5.1. Limitations of the roulette method

There are two situations where the roulette method should be applied with caution.

1. — Orbital phases of the test bodies are not independent. This happens if, for example, the satellites are in orbital resonances with each other and the phase-locking effect takes place, as is the case for planets in the outer solar system.
2. — The snapshot of the test bodies has a finite size comparable to the size of their orbits. Then there is a risk that the orbits extend beyond the snapshot boundary, and some bodies are observed preferentially near their pericenters just because they would not be seen otherwise. This bias to the pericenter can be significant only for satellites with highly eccentric orbits and it can be corrected: for each orbit reconstructed with a trial potential, one can check whether it extends beyond the snapshot boundary and calculate the fraction of the orbital period that the body spends beyond the boundary.

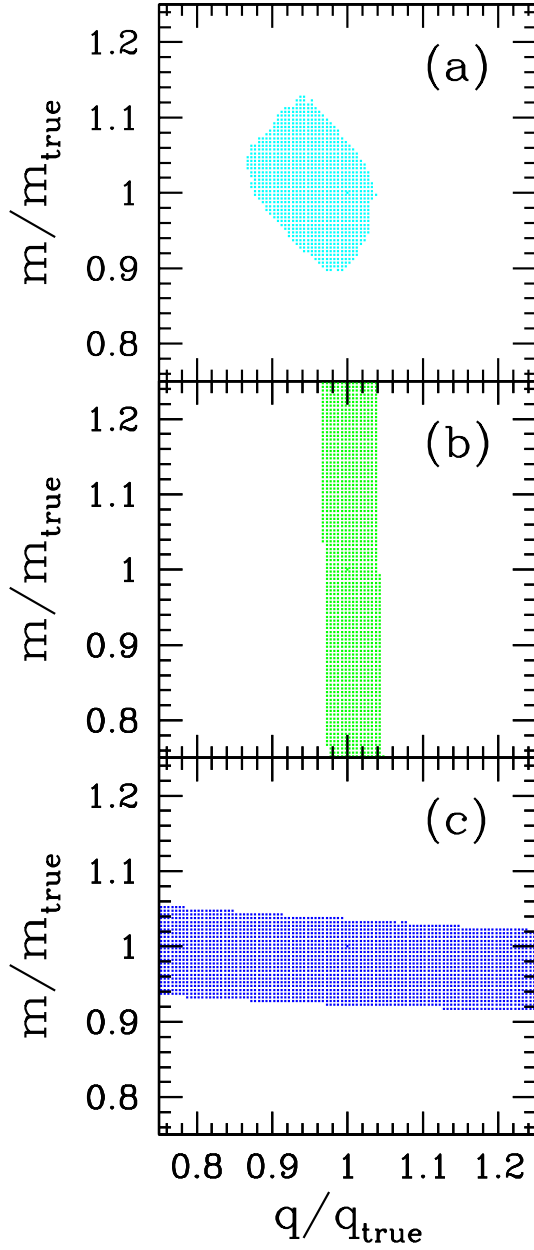


Fig. 8.— 90% confidence area on the $q - m$ plane obtained with the casino method for a Monte-Carlo generated data set of $N = 100$ bodies with random E and e . (a) E is drawn from the interval $E_0 < E < 0$. (b) E is drawn from $E_0 < E < (19/20)E_0$ (small orbits inside the halo). (c) E is drawn from $(E_0/20) < E < 0$ (large orbits outside the halo).

5.2. Applications

We briefly discuss below three astrophysical situations where the proposed method can be applied in its full 3D version developed in this paper.⁵

5.2.1. *The Oort limit*

The mass content of the Galactic disk in the solar neighborhood is inferred from the vertical motions of the nearby stars with respect to the galactic plane (see, e.g., chapt. 4.2 in Binney & Tremaine 1987). Mathematically, the problem reduces to a reconstruction of a one-dimensional potential $\Phi(z)$ from a snapshot of one-dimensional motions of N test bodies.

The Jeans equation was previously used to reconstruct $\Phi(z)$, which is not the most efficient method because it involves (arbitrary) binning of the data and numerical triple differentiation. Orbital roulette, in its full casino version, should be able to use the data optimally. It is expected to find $\Phi(z)$ that gives the stars random phases of vertical motion (roulette test), and the phases should be uncorrelated with the stars' orbital energies (card test). These conditions are necessary and sufficient for $\Phi(z)$ to be realistic.

5.2.2. *The mass of Sgr A**

Observations of stellar motions in the Galactic Center allow one to estimate the mass of the central dark object Sgr A*, which is believed to be a giant black hole (Genzel et. al. 2000; Schödel et. al. 2002, Ghez et. al. 2003). Normally, only sky-projected positions of stars are available, with the exception of a few tightly bound stars whose orbits have been partially mapped out.

By analyzing the data of Genzel et. al. (2000) we have recently found that the young stellar population in the Galactic center forms a thin disk (Levin & Beloborodov 2003). The inferred orientation of the disk plane was confirmed by further analysis of Genzel et. al. (2003). This finding gives a full 3D information for instantaneous motions of ten disk stars, which can be used to estimate the gravitational potential. We have applied the orbital roulette to these data and obtained a new independent estimate of the black hole mass (in preparation).

5.2.3. *Galactic potential probed by SIM*

Observations of satellites of our Galaxy constrain its gravitational potential and mass content. Within a decade, the Space Interferometry Mission (SIM) can provide the full 3-D information on

⁵We are grateful to Scott Tremaine who pointed out the applications outlined in §§ 5.2.1 and 5.2.3.

the motion of tens of the satellites, and the data should be used most efficiently.

The most advanced method to date, which is based on the Bayesian analysis, was developed by Little & Tremaine (1987) and Kochanek (1996). Little & Tremaine (1987) assumed that the satellites’ velocities are either radial or have isotropic distribution while Kochanek (1996) assumed some *à priori* form of the satellites’ distribution function. The orbital roulette, combined with the 3-D data, will alleviate the need for *à priori* assumptions. In the previous section we have demonstrated how our method estimates the mass and size of a spherically symmetric halo. A similar analysis can be done for the SIM data with a realistic model of the Galactic potential.

We thank Scott Tremaine for many helpful discussions. We also thank Mark Wilkinson, the referee, for his suggestions that helped improve the presentation of the paper. Both authors acknowledge financial support from NSERC. A.M.B. was supported by Alfred P. Sloan Foundation.

Appendix A: Keplerian orbits

A Keplerian orbit around point mass M is characterized by two integrals of motion: orbital energy and angular momentum,

$$E = \frac{v^2}{2} - \frac{GM}{r}, \quad \mathbf{l} = \mathbf{r} \times \mathbf{v}. \quad (33)$$

The semi-major axis a and eccentricity e of the orbit are given by

$$a = \frac{GM}{2|E|}, \quad 1 - e^2 = \frac{2|E|l^2}{G^2M^2}. \quad (34)$$

The pericenter and apocenter radii are

$$r_1 = a(1 - e), \quad r_2 = a(1 + e). \quad (35)$$

For the orbital roulette we need to determine the time of motion from r_1 to a given r . It is convenient to calculate the time using the relation

$$dt = \frac{dr}{v_r} = \left(\frac{2}{|E|} \right)^{1/2} r d\psi, \quad (36)$$

where ψ is defined by

$$\sin^2 \psi \equiv \frac{|E|(r - r_1)}{GM e}, \quad (37)$$

so that $r = r_1$ at $\psi = 0$ and $r = r_2$ at $\psi = \pi/2$. The full orbital period corresponds to ψ changing from 0 to π . The time of motion from a given r to r_1 is

$$t_p(r) = \frac{T}{\pi} \left(\psi - e \frac{\sin 2\psi}{2} \right), \quad (38)$$

where

$$T = 2t(r_1 \rightarrow r_2) = \frac{\pi GM}{\sqrt{2}|E|^{3/2}}. \quad (39)$$

is the orbital period. Time average of a magnitude Z over the orbit is given by

$$\langle Z \rangle = \frac{1}{T} \int_0^T Z dt = \frac{2}{T} \left(\frac{2}{|E|} \right)^{1/2} \int_0^{\pi/2} Z r d\psi. \quad (40)$$

Suppose an observed body has a measured position \mathbf{r} and velocity \mathbf{v} , and denote the angle between \mathbf{r} and \mathbf{v} by α . If we do not know the central mass M , the orbital parameters of the body and its phase $g = t_p(r)(T/2)^{-1}$ will depend on the assumed M or $x = GM/v^2 r$. In particular, we have

$$e(M) = \left[1 - \frac{(2x-1)}{x^2} \sin^2 \alpha \right]^{1/2}, \quad (41)$$

$$\sin^2 \psi(M) = \frac{x-1-xe}{2xe}, \quad (42)$$

$$g(M) = \frac{2}{\pi} \left(\psi - \frac{e}{2} \sin 2\psi \right), \quad (43)$$

$$\frac{dg}{dM} = \frac{1}{\pi e M x} \left[\frac{(1-e \cos 2\psi)}{\sin 2\psi} \left[1 - \left(1 - \frac{1}{x} \right)^2 \frac{\sin^2 \alpha}{e^2} \right] - \left(1 - \frac{1}{x} \right) \sin^2 \alpha \sin 2\psi \right]. \quad (44)$$

These expressions are used in section 3.5.

Appendix B: Isochron orbits

In contrast to the Keplerian case, we now have a characteristic scale b . It is convenient to use a dimensionless variable s instead of r ,

$$s = 1 + \sqrt{1 + \frac{r^2}{b^2}}, \quad r = b\sqrt{s(s-2)}. \quad (45)$$

The pericenter and apocenter radii are derived from the equation,

$$\frac{v_r^2}{2} = E - \Phi - \frac{l^2}{2r^2} = 0, \quad (46)$$

which gives

$$s_{1,2} = 1 + \frac{E_0}{E} \mp \left[\left(\frac{E_0}{E} - 1 \right)^2 + \frac{l^2}{2b^2 E} \right]^{1/2}. \quad (47)$$

Here $E_0 = \Phi(0) = -(Gm/2b)$ is the minimum possible energy for an orbit in the isochron potential. It is convenient to define a “semi-major” axis a in the s -space as

$$2a = b(s_1 + s_2 - 2) = \frac{Gm}{|E|}. \quad (48)$$

The relation between a and E is exactly the same as in the Keplerian case, and a has a normal Keplerian meaning at $a \gg b$. At $r < b$, however, the s -space a is very different; it can never be smaller than b and can be written as

$$a = b \frac{E_0}{E} > b. \quad (49)$$

Using $dt = dr/v_r$, one finds

$$dt = \frac{b}{2|E|} \frac{(s-1)ds}{\sqrt{(s_2-s)(s-s_1)}}. \quad (50)$$

Let us define angle ψ by

$$\sin^2 \psi = \frac{s-s_1}{s_2-s_1}. \quad (51)$$

Then the time of motion from a given r to the pericenter r_1 is

$$t_p(r) = \frac{T}{\pi} \left(\psi - e \frac{\sin 2\psi}{2} \right), \quad (52)$$

where T is the period of radial oscillations,

$$T = 2t(r_1 \rightarrow r_2) = \frac{\pi Gm}{\sqrt{2}|E|^{3/2}}, \quad (53)$$

and e is the “ s -space eccentricity” defined by

$$e = \frac{b(s_2-s_1)}{2a}. \quad (54)$$

The relation between E and T is the same as in the Keplerian case, and the formula for t_p is formally the same (although the eccentricity e is defined in the s -space here).

The eccentricity can also be expressed in terms of E and l ,

$$e^2 = \left(1 - \frac{E}{E_0} \right)^2 + \frac{l^2 E}{2b^2 E_0^2}. \quad (55)$$

Linear orbits with $l = 0$ have a maximum eccentricity

$$e_{\max}(E) = 1 - \frac{E}{E_0}. \quad (56)$$

In the limit $r \ll b$ (which corresponds to $\tilde{E} = E - E_0 \ll |E_0|$) the orbital motion occurs inside the homogeneous spherically-symmetric halo with density

$$\rho = \frac{3m}{16\pi b^3}. \quad (57)$$

REFERENCES

- Anderson, T. W., & Darling, D. A. 1952, *Ann. Math. Stat.*, 23, 193
- Bahcall, J. N., & Tremaine, S. 1981, *ApJ*, 244, 805
- Binney, J., & Tremaine, S. 1987, *Galactic Dynamics*, Princeton University Press, New Jersey
- Genzel, R., Pichon, C., Eckart, A., Gerhard, O. E., & Ott, T. 2000, *MNRAS*, 317, 348
- Genzel, R., et. al. 2003, *ApJ*, 594, 812
- Ghez, A. M., et. al. 2003, *ApJ*, 586, 127
- Kochanek, C. S. 1996, *ApJ*, 466, 638
- Kolmogorov, A. 1941, *Ann. Math. Stat.*, 12, 461
- Levin, Y., & Beloborodov, A. M. 2003, *ApJ*, 590, L33
- Little, B., & Tremaine, S. 1987, *ApJ*, 320, 493
- Navarro, J. F., Frenk, C. S., White, S. D. M. 1996, *ApJ*, 462, 563
- Page, T. 1952, *ApJ*, 116, 63
- Press, W. H., Flannery, B. P., Teukolsky, S., & Vetterling, W. 1992, *Numerical Recipes in C: The Art of Scientific Computing* (Cambridge: Cambridge Univ. Press)
- Schödel, R., et. al. 2002, *Nature*, 419, 694